IASSNS-AST 94/54

UDHEP-10-94

hep-ph 9410353

October 1994

Solar Neutrinos and the Principle of Equivalence

J.N. Bahcall[(a)], **P.I. Krastev**[(a) *] **and C.N. Leung**[(b)]

(a) School of Natural Sciences, Institute for Advanced Study

Princeton, NJ 08540

(b) Department of Physics and Astronomy, University of Delaware

Newark, DE 19716

Abstract

We study the proposed solution of the solar neutrino problem which requires a flavor nondiagonal coupling of neutrinos to gravity. We adopt a phenomenological point of view and investigate the consequences of the hypothesis that the neutrino weak interaction eigenstates are linear combinations of the gravitational eigenstates which have slightly different couplings to gravity, $f_1 G$ and $f_2 G$, $|f_1 - f_2| << 1$, corresponding to a difference in red-shift between electron and muon neutrinos, $\Delta z/(1+z) \sim |f_1 - f_2|$. We perform a χ^2 analysis of the latest available solar neutrino data and obtain the allowed regions in the space of the relevant parameters. The existing data

*Permanent address: Institute of Nuclear Research and Nuclear Energy, Bulgarian Academy of Sciences, BG–1784 Sofia, Bulgaria.

rule out most of the parameter space which can be probed in solar neutrino experiments, allowing only $|f_1 - f_2| \sim 3 \times 10^{-14}$ for small values of the mixing angle ($2 \times 10^{-3} \leq \sin^2(2\theta_G) \leq 10^{-2}$) and $10^{-16} \lesssim |f_1 - f_2| \lesssim 10^{-15}$ for large mixing ($0.6 \leq \sin^2(2\theta_G) \leq 0.9$). Measurements of the ^{8}B-neutrino energy spectrum in the SNO and Super-Kamiokande experiments will provide stronger constraints independent of all considerations related to solar models. We show that the recoil-electron spectrum measured by the Kamiokande-II collaboration can be used to exclude part of the allowed regions obtained above. We analyze the prospects of using future spectral measurements of solar neutrinos to distinguish the oscillation mechanism due to the violation of the equivalence principle from the conventional mechanisms which require neutrinos to have nondegenerate masses. We find that, for small mixing angles, these mechanisms lead to very different spectral predictions which will be distinguishable in the upcoming SNO and Super-Kamiokande experiments.

I. INTRODUCTION

Results from four solar neutrino experiments [1]- [4] utilizing different detection techniques consistently show a discrepancy between the measured ν_e flux from the sun and the ν_e flux predicted by various solar models [5]- [7]. Moreover, a comparison of two of the experiments suggests that, essentially independent of solar models, some new physical process may be changing the results of the neutrino energy spectrum [8]. The origin of this solar neutrino deficit is not yet known. A possible solution is neutrino flavor oscillations. The mechanism for neutrino oscillation originally proposed by Pontecorvo [9] assumes that neutrinos have nondegenerate masses and that the neutrino mass eigenstates are distinct from their weak interaction eigenstates. We shall refer to this as the mass mechanism. The most often discussed version of this type of solutions is the Mikheyev-Smirnov-Wolfenstein (MSW) effect [10], in which the solar electron neutrinos can be converted almost completely into muon or tau neutrinos due to the presence of matter in the Sun.

An alternative mechanism of neutrino oscillation which does not require neutrinos to have a nonzero mass was first proposed by Gasperini [11], and independently by Halprin and Leung [12], as a means to test the equivalence principle (EP). In this mechanism, neutrino oscillations occur as a consequence of an assumed flavor nondiagonal coupling of neutrinos to gravity which violates the EP. We shall refer to this as the VEP mechanism.

The VEP mechanism has been studied further in a number of papers [13]– [16]. One study [15] claims that this solution is already excluded by the data from the four solar neutrino experiments. On the other hand, a χ^2 analysis of the data performed in another study [13] reveals regions of the parameter space which are allowed by the results of all four solar neutrino experiments. One of our aims in the present paper is to address this controversy. We repeat the analysis using the most current solar neutrino data and find that, although strongly restricted by the data, this VEP mechanism is a phenomenologically allowed solution of the solar neutrino problem and deserves further study.

Having established the VEP mechanism as a possible solution to the solar neutrino

problem, it is necessary to find ways to determine whether the mass or the VEP mechanism is responsible for the observed solar neutrino deficit. We show that, because of their differing energy dependence, the two mechanisms yield, in the case of small mixing angles, very different and distinguishable predictions for spectral measurements in future solar neutrino experiments.

II. FORMALISM AND SOLUTIONS

We begin by recalling the important features of the two oscillation mechanisms. For simplicity, we only consider mixing of two neutrino flavors, e.g., ν_e and ν_μ. In the mass mechanism, the neutrino weak interaction (flavor) eigenstates, $\nu^{(W)} = (\nu_e, \nu_\mu)$, are assumed to be linear superpositions of the mass eigenstates, $\nu^{(M)} = (\nu_1^{(M)}, \nu_2^{(M)})$, with a mixing angle θ. The evolution equations for relativistic flavor neutrinos propagating in vacuum are given by

$$i\frac{d}{dr}\begin{pmatrix}\nu_e\\ \nu_\mu\end{pmatrix} = \frac{\Delta m^2}{2E}\begin{bmatrix}0 & \frac{1}{2}\sin 2\theta\\ \frac{1}{2}\sin 2\theta & \cos 2\theta\end{bmatrix}\begin{pmatrix}\nu_e\\ \nu_\mu\end{pmatrix}, \tag{1}$$

where E is the neutrino energy, $\Delta m^2 \equiv m_2^2 - m_1^2$, and $m_{1,2}$ are the mass eigenvalues. The survival probability for a ν_e after traveling a distance L is

$$P(\nu_e \to \nu_e) = 1 - \sin^2 2\theta \sin^2 \frac{\pi L}{\lambda_M}, \tag{2}$$

where λ_M is the oscillation length defined as

$$\lambda_M = \frac{4\pi E}{\Delta m^2}. \tag{3}$$

In the VEP mechanism neutrinos are assumed to be massless and there is no mass–dependent mixing.*. Instead the weak interaction eigenstates are assumed to be linear

*We do not consider explicitly the case of massive neutrinos in the VEP mechanism because this just complicates the analysis by introducing more parameters, but does not change the fundamental limits that are derived. See Ref. [16] for a recent discussion of this case.

superpositions of the gravitational interaction eigenstates, $\nu^{(G)} = (\nu_1^{(G)}, \nu_2^{(G)})$, with a mixing angle θ_G. It is further assumed that $\nu_1^{(G)}$ and $\nu_2^{(G)}$ interact with gravity with slightly different couplings, thus violating the EP and leading to neutrino oscillations when a neutrino propagates in a gravitational field. The neutrino evolution equations and the survival probability for a ν_e after traversing a distance L in the weak gravitational field of a static, spherical symmetric source are given (in the harmonic gauge) by Eqs. (1) and (2), with the substitutions [11] [12],

$$\theta \to \theta_G \quad \text{and} \quad \frac{\Delta m^2}{2E} \to 2E|\phi(r)|\Delta f, \tag{4}$$

where $\phi(r)$ is the Newtonian gravitational potential and $\Delta f \equiv f_2 - f_1$ is a measure of the degree of EP violation. Here $f_{1,2}$ can be identified as parameters in the parametrized post-Newtonian formalism [17] [18], and $f_1 = f_2$ if the EP is obeyed. In general relativity, $f_1 = f_2 = 1$.

There has been much discussion in the literature [19], mostly in the context of testing the EP in the $K^0 - \overline{K^0}$ system, as to whether the gravitational potential in Eq. (4) should include the potential of matter other than the Sun. If distant matter is included, then one obtains the counterintuitive result that the biggest effect is from material far away from the solar system. We adopt here the phenomenological point of view that the potential $\phi(r)$ is the difference between the Newtonian potential of the solar material at r and at $r = \infty$.

It is conceivable that the description of the violation of the equivalence principle outlined above will be modified if the violation is derived from a more rigorous theory, e.g., from string theory [20]. The dependence on the gravitational potential might be replaced in such a thory by a dependence on the gradient of the potential, which would eliminate the above-mentioned ambiguity concerning the relevant gravitational potential. For example, the term in Eq. (4) may be replaced by

$$2E|\phi(r)|\Delta f \to E\mathrm{R}_f|\nabla\phi| \tag{5}$$

where R_f is a dimensional parameter that describes the violation of the equivalence principle. The results obtained below for the VEP mechanism as defined in Eq. (4) can be easily

translated to the case represented by Eq. (5). Since $|\nabla\phi| \sim R_\odot^{-1}|\phi|$, where $R_\odot$ is the solar radius, we can interpret the numerical results for Δf in Eq. (4) as constraints on a mass scale for flavor violation,

$$\mathrm{M}_f \simeq (R_\odot \Delta f)^{-1} \tag{6}$$

It follows from the substitution (4) and Eq. (3) that the oscillation length in the VEP mechanism is, for a constant gravitational potential,

$$\lambda_G = \frac{\pi}{E|\phi|\Delta f} \tag{7}$$

Notice that λ_G is inversely proportional to the neutrino energy, whereas λ_M increases with E. It is this different energy dependence that leads to the observable distinction between the VEP and mass mechanisms.

Another consequence of this differing energy dependence is that, in contrast to the mass mechanism, the VEP mechanism cannot account for the observed solar neutrino deficit as the result of long-wavelength vacuum oscillations [13]. On the other hand, the solar neutrino data can be encompassed through the MSW mechanism [10] of resonance enhanced transitions in the sun [13]. For neutrinos propagating in matter, the evolution equations, Eq. (1), for the mass (VEP) mechanism are modified such that

$$\cos 2\theta_{(G)} \rightarrow \cos 2\theta_{(G)} - \frac{\sqrt{2}G_F N_e(r)}{2\pi/\lambda_{M(G)}} \tag{8}$$

where G_F is the Fermi constant and $N_e(r)$ is the electron number density inside the Sun. In the VEP case, the resonance occurs when

$$E = \frac{\sqrt{2}G_F N_e(r)}{2|\phi(r)|\Delta f \cos 2\theta_G} \tag{9}$$

An important ingredient in the analysis of resonant transitions in the Sun is the adiabaticity condition. For the VEP mechanism, it reads

$$\kappa = \frac{\sqrt{2}G_F \left(N_e\right)_{res} \tan^2 2\theta_G}{\left|\left(\frac{1}{N_e}\frac{dN_e}{dr}\right) - \left(\frac{1}{\phi}\frac{d\phi}{dr}\right)\right|_{res}} \gg 1. \tag{10}$$

For the mass mechanism, simply drop the $\phi^{-1}d\phi/dr$ term in the denominator and replace θ_G by θ. The dependence on the energy is implicit as the energy determines the resonant density via Eq. (9). Note that the adiabaticity condition in the VEP case is violated for low energy neutrinos whereas it is violated in the mass mechanism for high energy neutrinos.

It can be shown from Eqs. (1) and (8) that the probability amplitude ($A_e(r)$) of finding an electron neutrino at a distance r from where it was produced satisfies the equation,

$$A_e'' + A_e'(ia - b'/b) + b^2 A_e = 0, \tag{11}$$

where the prime symbols denote derivatives with respect to r. The parameters a and b are defined as

$$a = -\sqrt{2}G_F N_e(r) - 2E\phi(r)\Delta f \cos 2\theta_G, \tag{12}$$

$$b = -E\phi(r)\Delta f \sin 2\theta_G. \tag{13}$$

Eq. (11) is exactly solvable in the case of a Newtonian gravitational potential and zero electron density (e.g., outside the Sun). The general solution, expressed in terms of the dimensionless variable, $x = r/R_\odot$, has the form

$$A_e(x) = C_1 x^{iS\cos^2\theta_G} + C_2 e^{i\omega} x^{-iS\sin^2\theta_G}, \tag{14}$$

where C_1, C_2 and ω are real constants that have to be determined by the initial conditions. For a neutrino moving in the gravitational potential of the Sun, $S = 2E\Delta f G_N M_\odot$, where G_N is Newton's gravitational constant and $M_\odot$ is the solar mass. The probability to find a ν_e at a distance x, if at $x = 1$ a ν_e has been produced, is thus

$$P(x) = 1 - \sin^2(2\theta_G)\sin^2(\frac{S}{2}\ln(x)), \qquad x \geq 1. \tag{15}$$

By analogy with neutrino oscillations in vacuum one can introduce the oscillation length, $\mathrm{L}_G = 2\pi x R_\odot/S\ln(x)$, which turns out to be distance dependent. From (14) one can derive the average probability to obtain an electron neutrino at infinity given an arbitrary neutrino state at $r = R_\odot$:

$$\bar{P} = \cos^2 2\theta_G P(1) - \sin 2\theta_G \cos 2\theta_G R(1) + \frac{1}{2}\sin^2 2\theta_G. \tag{16}$$

Here $R(1) = Re[A_e(1)A_\mu^*(1)]$. This expression is necessary for the computation of the mean survival probabilities, especially in the case of large mixing angles, $\sin^2 2\theta_G \geq 0.1$, where one has to average over large-amplitude oscillations in vacuum between the Sun and the Earth. It is important also for the analysis in the long-wavelength regime where the oscillation length becomes comparable to the Earth-Sun distance. We have used these results to verify the finding in [13] that the possibility of a long-wavelength (or "just-so") VEP solution to the solar neutrino problem is ruled out by the present data.

The survival probability as a function of the product $E\Delta f$ is shown in Fig. 1 for a small as well as a large mixing angle. The curves in Fig. 1 have been obtained after averaging over the neutrino production regions [5] of the different components of the solar neutrino flux. The survival probabilities have been computed using the analytical result,

$$P = \frac{1}{2} + (\frac{1}{2} - P_{LZ})\cos 2\theta_G^o \cos 2\theta_G, \tag{17}$$

where $P_{LZ} = (e^{-\beta} - e^{-\alpha})/(1 - e^{-\alpha})$, with $\alpha = 2\pi\kappa\cos 2\theta_G/\sin^2 2\theta_G$ and $\beta = \frac{\pi}{2}\kappa(1 - \tan^2\theta_G)$. Here θ_G^o is the mixing angle at the production point of the neutrino. These expressions have been obtained by analogy with the ones in [21] for MSW-transitions in the mass mechanism. It is exact in the case of a density which varies exponentially with the distance, r, assuming that the variation of the gravitational potential with distance is much slower than the variation of the density with distance and can be neglected altogether. For small mixing angles this is an excellent approximation as the scale height of the gravitational potential is much larger than the density scale height. For example, the gravitational potential changes by a factor less than ten from the center of the Sun to the surface whereas the density changes by several orders of magnitude. We use the density distribution inside the Sun as given in [5] both for the electron number density and to compute the gravitational potential inside the Sun. For each value of $E\Delta f$ the gravitational potential has been put equal to the value it assumes at the point where the resonance takes place. We have verified by numerical

integration of the evolution equations that the results obtained with the analytical formula (17) are accurate to a few percent. In contrast with the mass mechanism, the adiabatic edge of the suppression pit in the case of VEP is at higher energies and, for small mixing angles, is bounded by the maximal density in the sun ($\approx 100 N_A$ cm^{-3}) to be at $E\Delta f \approx 10^{-12}$ MeV.

The resonance and adiabaticity conditions together determine the range of parameters which can be probed by solar neutrino experiments. This is depicted in Fig. 2 as the region bounded by the dotted lines. The horizontal line corresponds to a resonant density equal to the density in the center of the Sun for neutrinos with energy 0.2 MeV. For $\Delta f > 2 \times 10^{-12}$ there will be no resonance crossing in the Sun for neutrinos with energies higher than 0.2 MeV. Oscillations with an amplitude $\sim \sin^2 2\theta_G$ will still take place, however, the oscillation length at the Earth for neutrinos of energies 0.1 MeV and higher will be smaller than 10^{-4}R$_\odot$. Therefore the averaging over the distance between the source and detector will result in energy independent suppression of all solar neutrino fluxes, which does not give an acceptable fit to the data. The diagonal line in Fig. 2 corresponds to $\kappa = 1$ for neutrinos of energy 10 MeV. For values of $\sin^2 2\theta_G$ and Δf in the region below this line the transitions are strongly nonadiabatic and cannot account for the solar neutrino problem.

III. COMPARISON WITH DATA

In section III-A we show which regions of the parameter space for the VEP mechanism are ruled out by the measured counting rates in the four operating solar neutrino experiments. In section III-B we use the implied spectral distribution of the ^{8}B-neutrino spectrum and the existing Kamiokande measurements to further reduce the allowed parameter space. We also show in Section III-B, and especially Figures 3 and 4, how future spectral measurements with SNO and Super-Kamiokande can be used to distinguish between different mechanisms for solving the solar neutrino problem.

A. Rates

We use the following recent experimental results: $Q_{Cl} = (2.55 \pm 0.25) SNU$ [1], $\Phi_K(^8B) = (2.89 \pm 0.41) \times 10^6$ cm^{-2}s^{-1} [2], $Q_{Ga} = (73 \pm 19.3) SNU$ [3], and $Q_{Ga} = (79 \pm 11.7) SNU$ [4].

In our χ^2 analysis of the latest solar neutrino data in terms of the "MSW-enhanced" VEP mechanism we have adopted a procedure that takes into account the theoretical uncertainties in the standard solar model as described in [22]. The analysis yields two allowed regions at 95 % C.L., a "small mixing region" for: $2 \times 10^{-3} \leq \sin^2(2\theta_G) \leq 10^{-2}$ and $2.7 \times 10^{-14} \leq \Delta f \leq 3.3 \times 10^{-14}$; and a "large mixing region" for: $0.6 \leq \sin^2(2\theta_G) \leq 0.9$ and $1.0 \times 10^{-16} \leq \Delta f \leq 1.5 \times 10^{-15}$. These are shown in Fig. 2 by the unhatched regions within the solid curves. The quality of the fit is better for the small mixing solution where $\chi^2_{min} = 0.31$. For two degrees of freedom (four experiments – two parameters fitted), this is a very good fit comparable to the case of the MSW solution in the mass mechanism where $\chi^2_{min} = 0.12$ (see [23]). For the large mixing angle solution the fit is considerably worse with $\chi^2_{min} = 3.4$. The allowed regions shown in Fig. 2 are compatible with the ones found in [13]. The differences can be attributed to the more recent experimental data used in the present analysis as well as to the different ways in which these data were treated.

We have repeated our analysis of the data by including the gravitational field of the local supercluster which is estimated by Kenyon [19] to be 3×10^{-5}. This potential, being three times the gravitational potential of the Sun at its center, would dominate. The allowed regions in this case change little in shape but are shifted to lower values of Δf by approximately a factor of three. The small mixing allowed region is shifted also to smaller angles ($1.5 \times 10^{-3} \leq \sin^2(2\theta_G) \leq 6.0 \times 10^{-3}$) as the stronger gravitational field improves adiabaticity if all the other parameters in Eq. (10) remain the same. The improved adiabaticity results in a broader suppression pit in the survival probability and the pp-neutrinos become more strongly suppressed for the same values of $\sin^2 2\theta_G$, which comes into conflict with the results from the Gallium experiments.

Different components of the solar neutrino flux are suppressed differently in the two

allowed regions. In the large mixing region the pp-, ^{7}Be-, ^{8}B-, pep-, and CNO-neutrinos are suppressed almost equally because the allowed Δf values correspond to the flat bottom part of the survival probability curve (see Fig. 1b). On the other hand, in the region of small mixing, the ^{7}Be-neutrinos are suppressed more strongly than the rest of the solar neutrinos as they are at the deepest part of the narrow suppression pit. This is similar to the analogous regions in the case of a MSW solution for the mass mechanism. However, there is an important difference between the two cases, namely, the energy ranges corresponding to adiabatic and nonadiabatic transitions are opposite. It is this difference which leads to different neutrino spectra for the two cases. The nonadiabatic edge in the case of the mass mechanism is not as steep as the adiabatic edge in the case of the VEP mechanism. Since these are responsible for the spectral distortion of the boron neutrinos one expects more abrupt changes of this spectrum in the case of VEP.

B. Spectral Distortion

It has been shown in [24] that the solar neutrino spectrum is independent of all solar model considerations to a very high accuracy. Distortions of the spectra, if found experimentally, would constitute a strong evidence for a neutrino physics solution of the solar neutrino problem.

The Kamiokande-II (K-II) collaboration has obtained the first piece of spectral information on solar neutrinos by measuring the energy spectrum of the recoil electrons from neutrino-electron scattering [25]. Because of the relatively large statistical errors, the constraints on possible distortions of the spectrum are not very stringent. We have used the K-II data to rule out values of the parameters Δf and $\sin^2 2\theta_G$. The excluded region at 95 % C.L. is shown as the hatched region in Fig. 2. This exclusion is obtained by comparing the predicted recoil–electron spectrum with the measured one for a large number of values for Δf and $\sin^2 2\theta_G$, taking into account the energy resolution and threshold efficiency function of the K-II detector. The excluded region overlaps with part of the allowed "small

mixing region" obtained from the χ^2 analysis of the event rates discussed above. It should be emphasized that, while the position and shape of the allowed regions in Fig. 2 depend on the predicted solar neutrino flux from the standard solar model, the region excluded by the recoil-electron spectrum is solar model independent.

The excluded region in Fig. 2 depends sensitively on the highest energy data point in the K-II spectrum. This point has a relatively small error bar which is a result of combining the data from all higher-energy bins above 13 MeV. If this data point is ignored, we find that the excluded region will be reduced considerably and will no longer overlap with the allowed region. The situation will be improved when more precise measurements of the recoil-electron spectrum become available from the upcoming SNO and Super-Kamiokande detectors.

We have studied the possibility of using the SNO and Super-Kamiokande measurements to identify the mixing mechanism responsible for the solar neutrino problem. We show in Fig. 3 the predicted spectra for various allowed values of the mixing parameters. Spectra predicted for MSW transitions in the VEP mechanism and in the mass mechanism are displayed in Fig. 3a and Fig. 3b, respectively. What is actually shown is the ratio of the predicted spectrum, $\mathrm{F(T_e)}$, to the corresponding spectrum, $\mathrm{F_{st}(T_e)}$, calculated for the standard solar model [5] with no neutrino mixing. We normalize the value of this ratio such that it is equal to 1 for recoil-electrons with energy $T_e = 10$ MeV. For large mixing angles, there is little distortion from the standard solar model spectrum, both for the VEP and for the mass mechanism. This is why the measured K-II spectrum only excludes a region corresponding to small mixing angles (see Fig. 2). On the other hand, the spectral distortion for small mixing angles in the VEP case is noticeably different from that in the mass mechanism.

One possible measure of the difference in the spectral distortion is the derivative,

$$\xi_e(\mathrm{T_e}) = \frac{\mathrm{d}}{\mathrm{dT_e}} \left[\frac{\mathrm{F(T_e)}}{\mathrm{F_{st}(T_e)}} \right] \tag{18}$$

As an illustration of the sensitivity of this variable to the distortions of the shape of the spectral curves we have compared its values for the VEP and mass mechanisms at $\mathrm{T_e} =$

10 MeV. For the VEP mechanism $\xi_e(10\ \text{MeV})$ is equal to 0.31, 0.29 and 0.27 MeV^{-1} for curves labeled from 1 to 3 in Fig. 3a. In the case of the mass mechanism the corresponding values are 0.036, 0.035 and 0.044 MeV^{-1} for curves labeled 4 to 6 in Fig. 3b. For the rest of the curves shown in these two figures the derivative is very close to zero, typically an order of magnitude smaller than the above values.

Since long-wavelength vacuum oscillation for the mass mechanism is still a possible solution to the solar neutrino problem, it is necessary to also study the calculated recoil-electron spectra for this case, which are shown in Fig. 3c. We see that the spectral distortion here can be as large as that in the VEP mechanism. However, the character of this distortion is different. For curves labeled from 1 to 6 in Fig. 3c the corresponding values of $\xi_e(10\ \text{MeV})$ are – 0.156, 0.0094, 0.057, 0.10, 0.089 and 0.0695 MeV^{-1}. Furthermore, at energies below 10 MeV the general behavior of the spectral distortion is drastically different in the two cases. Therefore future solar neutrino experiments should be able to distinguish, independent of solar model predictions of the neutrino fluxes, between the different scenarios by comparing the shapes of the recoil–electron spectra, provided the experimental uncertainties are sufficiently small.

In addition to neutrino-electron scattering, the SNO detector can also detect the ^{8}B-neutrinos from the Sun by the process $\nu_e + d \rightarrow p + p + e^-$. In the case of the MSW effect for the mass mechanism the ^{8}B-neutrino spectrum is smoothly and almost uniformly distorted in the region between 5 and 14.5 MeV, which is the interval of energies to which the SNO detector is expected to be sensitive. On the other hand, in the case of the VEP mechanism, the distortion of the ^{8}B-neutrino spectrum is much more abrupt in the small mixing region. This is illustrated in Figs. 4a and 4b where the ^{8}B-neutrino spectra are shown in the two cases for sets of allowed parameters. Similar to Fig. 3, the spectra are normalized to the standard ^{8}B-neutrino spectrum (corresponding to no neutrino mixing) and to their values at 10 MeV. It is evident from these figures that, for small mixing angles, the deviations from the standard ^{8}B-neutrino spectrum are large. Moreover, the spectral distortions in the case of the VEP mechanism are strikingly different from the corresponding ones in the case of

the MSW solution for the mass mechanism. The derivative, $\frac{\mathrm{d}}{\mathrm{dE}_\nu}\,[\mathrm{F}(\mathrm{E}_\nu)/\mathrm{F}_{\mathrm{st}}(\mathrm{E}_\nu)]$, has values 1.1, 1.0 and 0.90 at $E_\nu = 10$ MeV for curves 1 to 3 in Fig. 4a, whereas it is equal to 0.10, 0.093 and 0.10 for curves 4 to 6 in Fig. 4b. The difference in the shape of these curves is big enough to be measured in the SNO detector as indicated by the estimated error bars after five years of operation of this detector.†

We also compare the VEP spectra with those predicted for the mass mechanism in the case of long-wavelength vacuum oscillations, displayed in Fig. 4c. The values of the corresponding derivative at $E_\nu = 10$ MeV are – 0.43, – 0.16, 0.070, 0.23, 0.21 and 0.19 MeV^{-1} for curves labeled 1 to 6 in Fig. 4c. We see again a measurable difference between the spectra in these two cases. The neutrino oscillations in vacuum result in stronger distortions in the lower spectrum of the energy interval between 5 and 14.5 MeV whereas the VEP distortions are more prominent at the higher energies.

IV. CONCLUSION

Using the current solar neutrino data, we find that the VEP mechanism remains a viable solution to the solar neutrino problem. The existing data rule out a possible violation of the principle of equivalence for a substantial region of the Δf - $\sin^2 2\theta_G$ plane between $10^{-18} < \Delta f < 10^{-12}$. This result is much stronger than the constraints obtained from SN1987A by comparing the arrival times of neutrinos and photons, $|f_\nu - f_\gamma| < 3 \times 10^{-3}$ [27] [28], and by comparing neutrinos with anti-neutrinos, $|f_\nu - f_{\bar{\nu}}| < 10^{-6}$ [29] [30]. It is also stronger than the best limit of 10^{-12} derived from torsion balance experiments [31], which refers to macroscopic samples of matter and not to neutrinos. Consequently, the violation of the equivalence principle by neutrinos, indicated by the allowed regions in Fig. 2, does not translate into a violation of the equivalence principle by the charged leptons at an

†Efficiency and energy resolution have not been included in the estimate of the error bars. The error bars are simply the square root of the estimated number of events per year.

unacceptable level. For example, it does not induce lepton flavor changing transitions such as $\mu \to e\gamma$ at a rate already excluded by experiment [18].

If the violation of the equivalence principle has the gradient form given in Eq. (5) rather than the linear form in Eq. (4), then from Eq. (6) and the limits cited above for Δf, we conclude that a significant fraction of flavor-violating couplings in the range 10^{-3} eV $\lesssim$ M_f $\lesssim$ 10^3 eV are excluded.

Observation of the distortion of the solar neutrino spectrum would be a strong indication that neutrino physics is at the heart of the solar neutrino problem. We have shown that the recoil-electron spectrum measured by Kamiokande-II excludes, in a solar model independent way, a region of the otherwise allowed VEP parameter space. We have studied the prospects of using spectral measurements of solar neutrinos to distinguish among various neutrino oscillation mechanisms. In the case of small mixing angles, spectral measurements from upcoming solar neutrino experiments will be able to determine which is the underlying mechanism of neutrino mixing. On the other hand, atmospheric neutrino data favor large mixing, in which case spectral measurements of solar neutrinos cannot easily distinguish the VEP mechanism from the mass mechanism. In this case, long-baseline accelerator neutrino experiments [13] [14] with typical neutrino energies between 1 and 20 GeV and separations of order hundreds of kilometers may provide the means to distinguish these two mechanisms.

Acknowledgements

We are grateful to A. M. Polyakov for an informative and stimulating discussion of possible mechanisms for the violation of the equivalence principle in string theories. The work of P.I.K. has been partially supported by Dyson Visiting Professor Funds from the Institute for Advanced Study. He would like to thank the Theory Group at Fermilab and C.N.L. thanks the International School for Advanced Studies, especially S. T. Petcov, for

their hospitality during the latter stage of this work. C.N.L. also wishes to thank S. T. Petcov and A. Yu Smirnov for useful discussions. This work is supported in part by the U.S. Department of Energy under Grants No. DE–FG05–85ER–40219 and No. DE-FG02-84ER40163 and by the North Carolina Supercomputing Program.

REFERENCES

[1] R. Davis, D.S. Harmer and K.C. Hoffman, Phys. Rev. Lett. **20**, 1205 (1968); R. Davis, in Proc. of the 21st Int. Cosmic Ray Conf., ed. by R.J. Protheroe (University of Adelaide Press 1990), p. 143

[2] Kamiokande II Collaboration, K. Hirata *et al.*, Phys. Rev. Lett. **65**, 1297 (1990); **65**, 1301 (1990); Phys. Rev. D **44**, 2241 (1991).

[3] SAGE Collaboration, J.N. Abdurashidov *et al.*, Phys. Lett. B **328** (1994) 234, A.I. Abazov *et al.*, Phys. Rev. Lett. **67**, 3332 (1991); T. Bowles, talk presented at NEUTRINO'92, Granada, Spain.

[4] GALLEX Collaboration, P. Anselmann *et al.*, Phys. Lett. B **327**, 377 (1994), **314**, 445 (1993), **285**, 376 (1992); **285**, 390 (1992).

[5] J. N. Bahcall and M. M. Pinsonneault, Rev. Mod. Phys. **64**, 885 (1992).

[6] J. N. Bahcall and R. K. Ulrich, Rev. Mod. Phys. **60**, 297 (1989).

[7] S. Turck-Chieze and I. Lopez, Astrophys. J. **408**, 347 (1993); S. Turck-Chieze *et al.*, Phys. Rep. **230**, 57 (1993).

[8] J.N. Bahcall and H. Bethe, Phys. Rev. D **47**, 1298 (1993); Phys. Rev. Lett. **65**, 2233 (1990).

[9] B. M. Pontecorvo, Sov. Phys. JETP **34**, 247 (1958).

[10] L. Wolfenstein, Phys. Rev. D **17**, 2369 (1978); Phys. Rev. D **20**, 2634 (1979). S. P. Mikheyev and A. Yu Smirnov, Yad. Fiz. **42**, 1441 (1985) [Sov. J. Nucl. Phys. **42**, 913 (1985)]; Nuovo Cim. **C9**, 17 (1986).

[11] M. Gasperini, Phys. Rev. D **38**, 2635 (1988); Phys. Rev. D **39**, 3606 (1989).

[12] A. Halprin and C.N. Leung, Phys. Rev. Lett. **67** (1991) 1833; Nucl. Phys. B (*Proc. Suppl.*) **28A**, 139 (1992).

[13] J. Pantaleone, A. Halprin and C. N. Leung, Phys. Rev. D **47**, R4199 (1993).

[14] K. Iida, H. Minakata and O. Yasuda, Mod. Phys. Lett. **A 8**, 1037 (1993).

[15] M.N. Butler, S. Nozawa, R. Malaney and A.I. Boothroyd, Phys. Rev. D **47**, 2615 (1993).

[16] H. Minakata and H. Nunokawa, preprint TMUP-HEL-9402 (April, 1994).

[17] A. Halprin, C. N. Leung and J. Pantaleone, talk presented by A. Halprin at the 14th International Workshop on Weak Interactions and Neutrinos, Seoul, Korea, 19 - 24 July, 1993.

[18] A. Halprin, C.N. Leung and J. Pantaleone, in preparation

[19] P. Morrison, Am. J. Phys. **26**, 358 (1958); M. L. Good, Phys. Rev. **121**, 311 (1961); I. R. Kenyon, Phys. Lett. B **237**, 274 (1990); R. J. Hughes and M. H. Holzscheiter, J. Mod. Opt. **39**, 263 (1992); R. J. Hughes, Phys. Rev. D **46**, R2283 (1992).

[20] For a recent discussion of the violation of the equivalence principle in superstring theories, see T. Damour and A. M. Polyakov, Nucl. Phys. B **423**, 532 (1994).

[21] S.T. Petcov, Phys. Lett. B **200**, 373 (1988); *ibid.* **214**, 139 (1988); see also Nucl. Phys. B (Suppl.) **13**, 527 (1990).

[22] N. Hata and P. Langacker, Phys. Rev. D **50**, 632 (1994).

[23] P.I. Krastev and S.T. Petcov, "Testing the Vacuum Oscillation and the MSW Solutions of the Solar Neutrino Problem", preprint FERMILAB–PUB–94/188–T, July 1994, hep-ph/9408234.

[24] J.N. Bahcall, Phys. Rev. D **44**, 1644 (1991).

[25] K.S. Hirata *et al.*, Phys. Rev. Lett. **65**, 1301 (1990).

[26] K.S. Hirata *et al.*, Phys. Rev. D **44**, 2241 (1991).

[27] M.J. Longo, Phys. Rev. Lett. **60**, 173 (1988).

[28] L. M. Krauss and S. Tremaine, Phys. Rev. Lett. **60**, 176 (1988).

[29] J.M. LoSecco, Phys. Rev D **38**, 3313 (1988).

[30] S. Pakvasa., W. A. Simmons and T. J. Weiler, Phys. Rev. D **39**, 1761 (1989).

[31] V. B. Braginsky and V. I. Panov, Sov. Phys. JETP **34**, 463 (1972).

Figure Captions

Fig.1 Survival probabilties as a function of $E\Delta f$ for: a) $\sin^2 2\theta_G = 5 \times 10^{-3}$ and b) $\sin^2 2\theta_G = 0.8$. The different curves correspond to averaging over the different neutrino production regions according to the solar model in [5].

Fig.2 95 % C.L. allowed regions of the parameters Δf and $\sin^2 2\theta_G$ derived from the latest solar neutrino data (unhatched). The region that can be probed with solar neutrino experiments is bounded by the dotted lines. The hatched region is ruled out by the recoil–electron energy spectrum measured by the Kamiokande–II collaboration.

Fig.3 Ratios of the predicted recoil-electron spectra for: a) "MSW–enhanced" VEP mechanism, b) MSW effect in the mass mechanism, and c) neutrino oscillations in vacuum (note the different scale in each of these cases) to the standard spectrum of recoil-electrons from boron neutirnos. T_e is the recoil-electron energy. The chosen values of the parameters for each case correspond to values allowed by the current solar neutrino data.

Fig.4 Predicted ratios of ^{8}B-neutrino spectra to the standard boron neutrino spectrum for the same three cases as in Fig. 3. Note the different scale used in each case. E_ν is the neutrino energy.

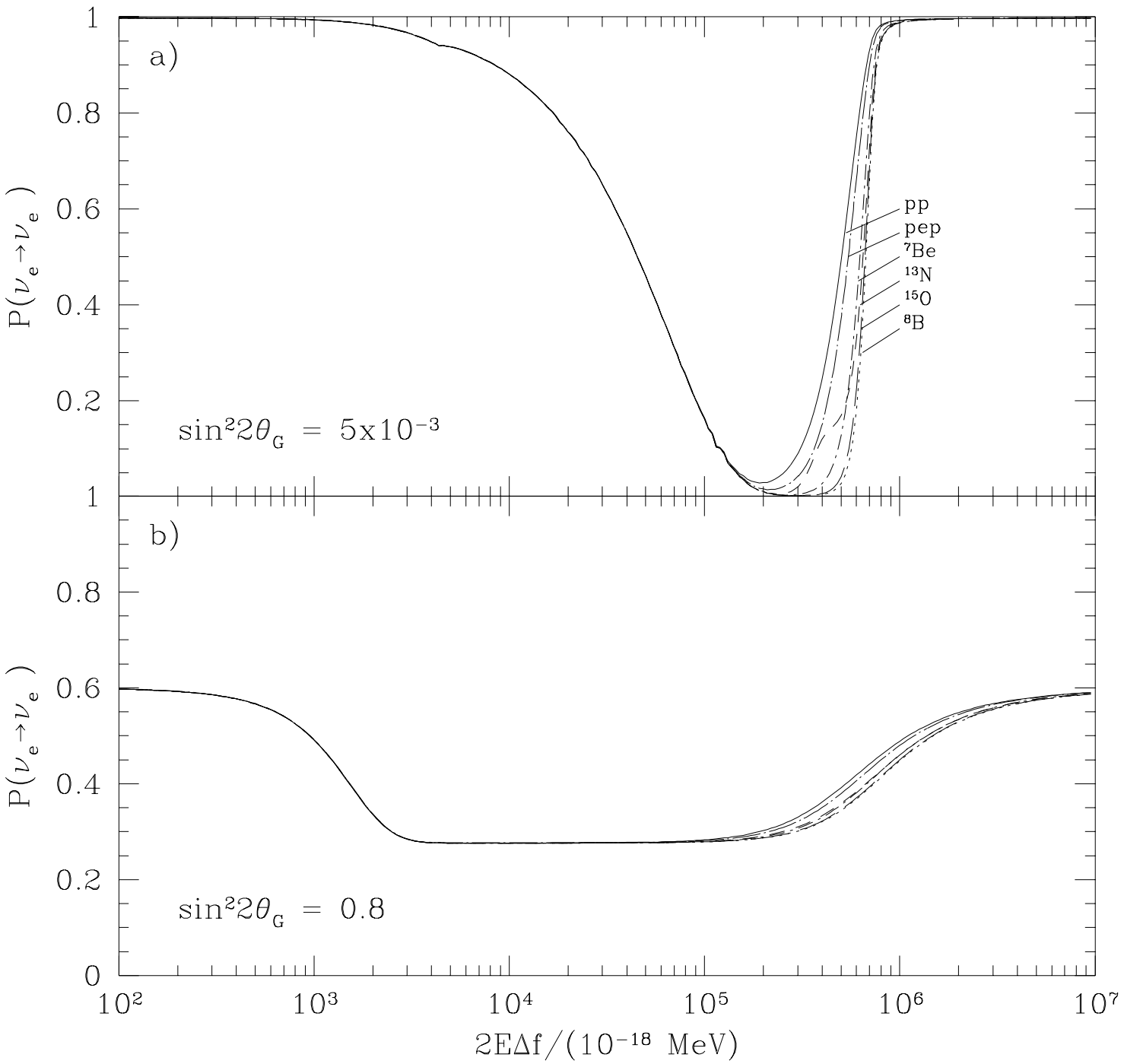
a)
b)
pp
pep
^{7}Be
^{13}N
^{15}O
^{8}B
$\sin^2 2\theta_G = 5\times10^{-3}$
$\sin^2 2\theta_G = 0.8$
$P(\nu_e \to \nu_e)$
$2E\Delta f/(10^{-18}$ MeV)
1
0.8
0.6
0.4
0.2
0
10^2
10^3
10^4
10^5
10^6
10^7

Fig.1

This figure "fig1-1.png" is available in "png" format from:

http://arXiv.org/ps/hep-ph/9410353v1

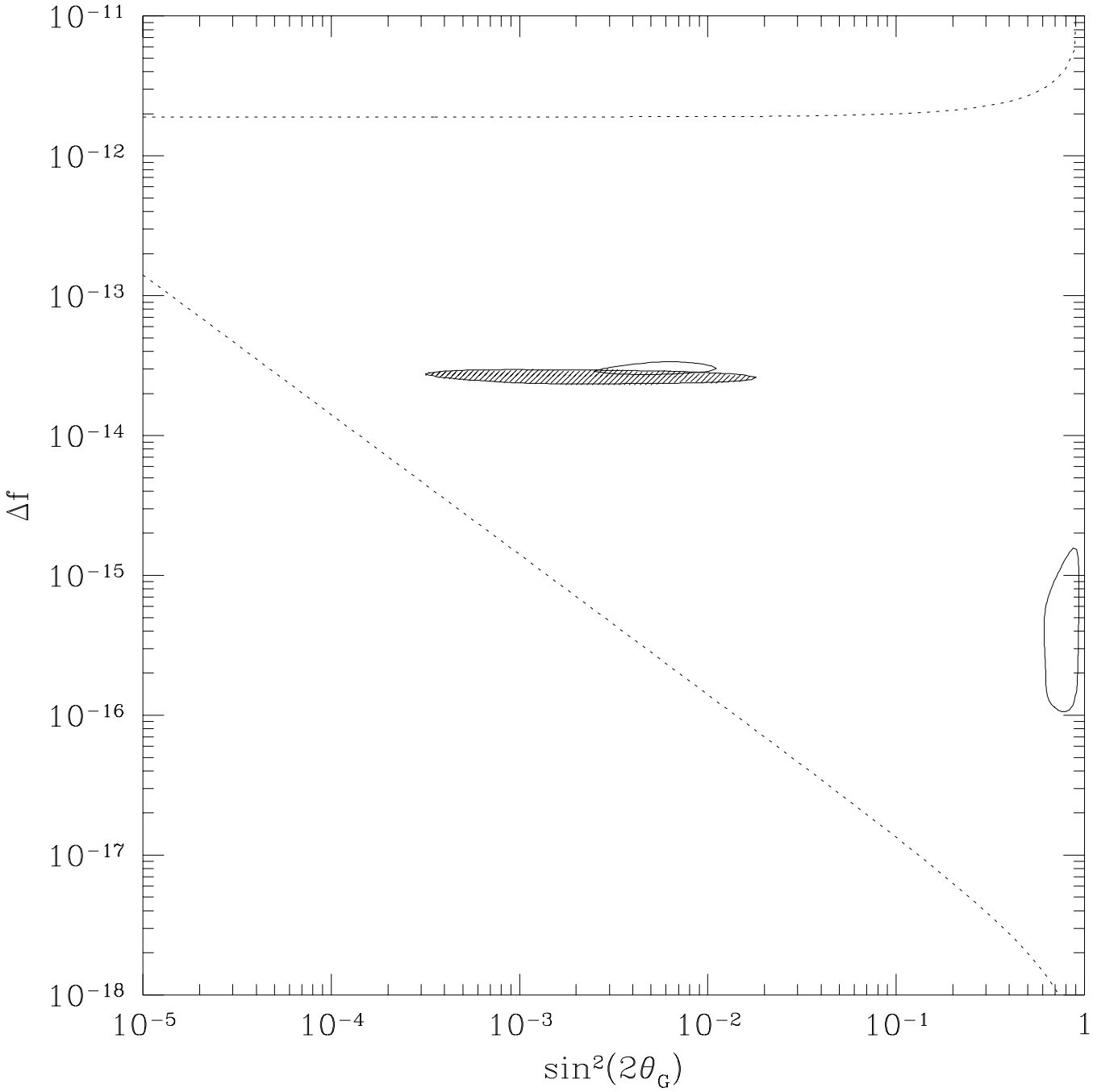
10^{-11}
10^{-12}
10^{-13}
10^{-14}
10^{-15}
10^{-16}
10^{-17}
10^{-18}
Δf
10^{-5}
10^{-4}
10^{-3}
10^{-2}
10^{-1}
1
$\sin^2(2\theta_G)$

Fig.2

This figure "fig1-2.png" is available in "png" format from:

http://arXiv.org/ps/hep-ph/9410353v1

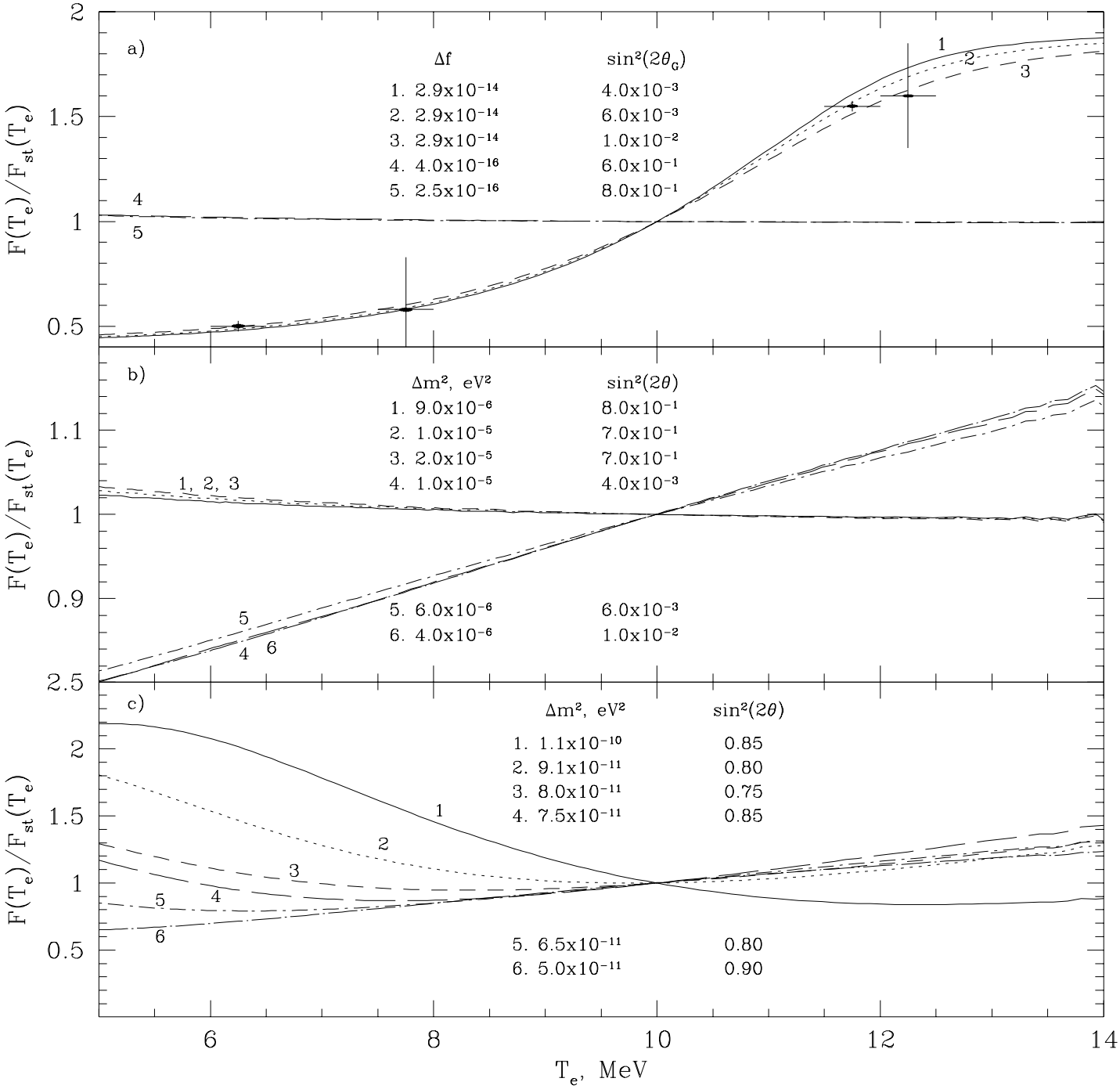
a)
Δf
sin²(2θ_G)
1. 2.9x10⁻¹⁴ 4.0x10⁻³
2. 2.9x10⁻¹⁴ 6.0x10⁻³
3. 2.9x10⁻¹⁴ 1.0x10⁻²
4. 4.0x10⁻¹⁶ 6.0x10⁻¹
5. 2.5x10⁻¹⁶ 8.0x10⁻¹
b)
Δm², eV²
sin²(2θ)
1. 9.0x10⁻⁶ 8.0x10⁻¹
2. 1.0x10⁻⁵ 7.0x10⁻¹
3. 2.0x10⁻⁵ 7.0x10⁻¹
4. 1.0x10⁻⁵ 4.0x10⁻³
5. 6.0x10⁻⁶ 6.0x10⁻³
6. 4.0x10⁻⁶ 1.0x10⁻²
c)
Δm², eV²
sin²(2θ)
1. 1.1x10⁻¹⁰ 0.85
2. 9.1x10⁻¹¹ 0.80
3. 8.0x10⁻¹¹ 0.75
4. 7.5x10⁻¹¹ 0.85
5. 6.5x10⁻¹¹ 0.80
6. 5.0x10⁻¹¹ 0.90
F(T_e)/F_st(T_e)
T_e, MeV

Fig.3

This figure "fig1-3.png" is available in "png" format from:

http://arXiv.org/ps/hep-ph/9410353v1

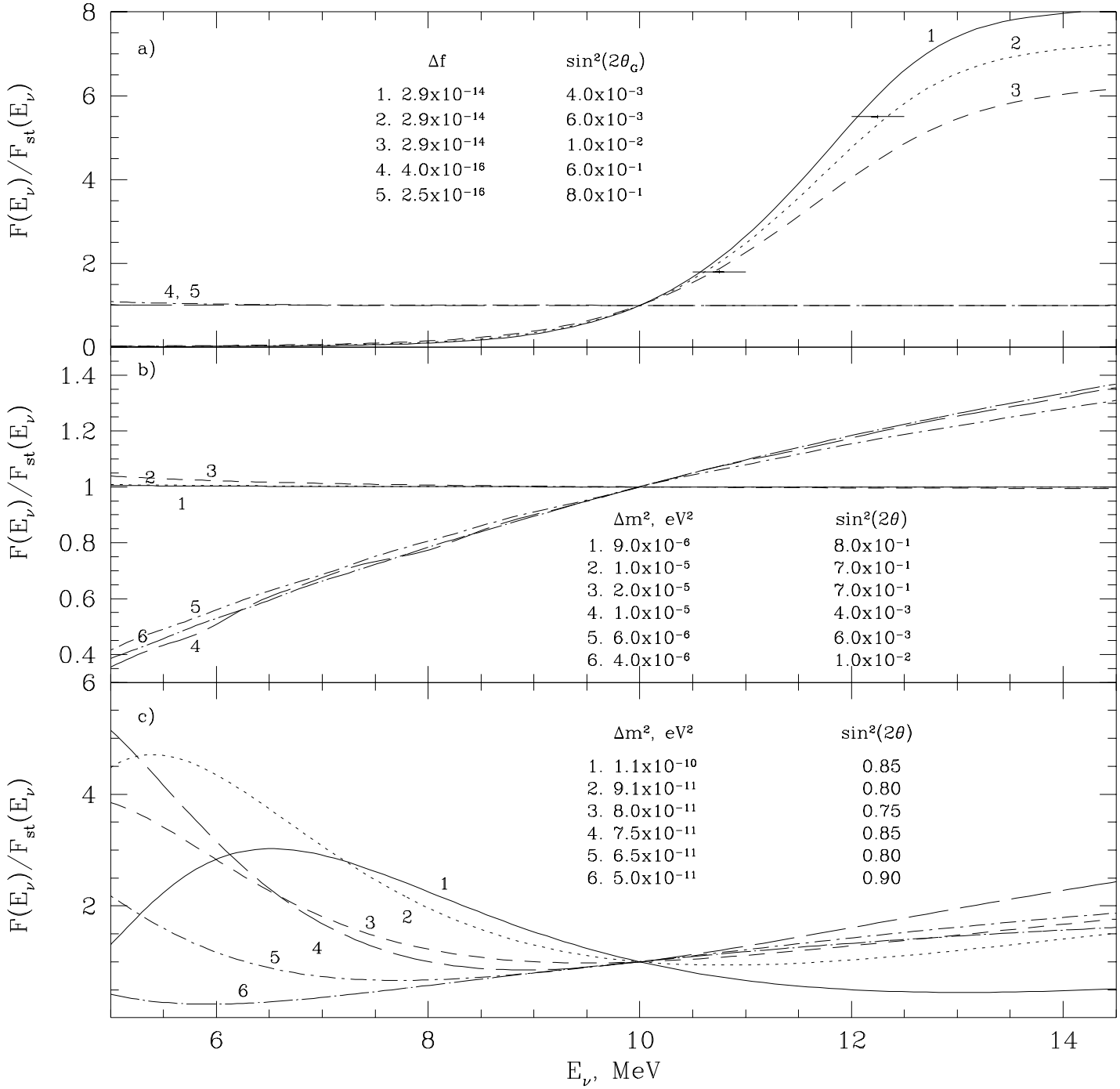
a)
Δf
sin²(2θ_G)
1. 2.9x10⁻¹⁴ 4.0x10⁻³
2. 2.9x10⁻¹⁴ 6.0x10⁻³
3. 2.9x10⁻¹⁴ 1.0x10⁻²
4. 4.0x10⁻¹⁶ 6.0x10⁻¹
5. 2.5x10⁻¹⁶ 8.0x10⁻¹
1
2
3
4, 5
b)
Δm², eV²
sin²(2θ)
1. 9.0x10⁻⁶ 8.0x10⁻¹
2. 1.0x10⁻⁵ 7.0x10⁻¹
3. 2.0x10⁻⁵ 7.0x10⁻¹
4. 1.0x10⁻⁵ 4.0x10⁻³
5. 6.0x10⁻⁶ 6.0x10⁻³
6. 4.0x10⁻⁶ 1.0x10⁻²
c)
Δm², eV²
sin²(2θ)
1. 1.1x10⁻¹⁰ 0.85
2. 9.1x10⁻¹¹ 0.80
3. 8.0x10⁻¹¹ 0.75
4. 7.5x10⁻¹¹ 0.85
5. 6.5x10⁻¹¹ 0.80
6. 5.0x10⁻¹¹ 0.90
F(E_ν)/F_st(E_ν)
E_ν, MeV

Fig.4

This figure "fig1-4.png" is available in "png" format from:

http://arXiv.org/ps/hep-ph/9410353v1